Improved Myocardial Tagging Contrast

S. E. Fischer, G. C. McKinnon, S. E. Maier, P. Boesiger

Myocardial tagging is a new noninvasive MRI method that allows the study of myocardial motion with high accuracy. However, with conventional tagging techniques tagging contrast is impaired at later heart phases due to longitudinal relaxation. An improved method, called Complementary SPAtial Modulation of Magnetization (CSPAMM), which separates the component of the magnetization with the tagging information from the relaxed component by subtraction of two measurements with first a positive and then a negative tagging grid, is presented. This technique improves the grid contrast and greatly facilitates the automatic evaluation of the myocardial motion. Thus the motion assessment of the entire heart cycle becomes possible. The improvements are documented by numerical simulations and by experiments on phantoms and on human volunteers.

Key words: myocardial tagging; SPAMM; cardiac motion; heart motion analysis.

INTRODUCTION

There is an increasing interest in noninvasive myocardial motion studies of patients suffering from different kinds of heart diseases, such as aorta stenosis, hypertrophic cardiomyopathy, or myocardial infarction. Based on the property of nuclear magnetic resonance imaging that a region with presaturated magnetization is fixed with respect to the tissue, a method has been proposed (1), which allows one to evaluate the motion of the myocardium by following the deformation of saturated stripes in conventional MR images. An important extension postulated by Axel and Dougherty (2, 3), called spatial modulation of the magnetization or SPAMM, can be used to generate a two-dimensional grid of stripes of saturated spins, a so-called tagging grid. Usually this grid is applied immediately after the R-wave (using ECG-triggering) in the end diastolic heart phase, preceding the acquisition of a set of images at different phases of the heart cycle. The tagging grid is induced by the application of a sequence of binomial RF pulses interspersed with weak dephasing gradients. The application of this grid permits a highly accurate quantification of the two dimensional myocardial motion in a slice.

With the conventional SPAMM technique followed by a multiheart phase imaging sequence, the problem arises that the tagging contrast at later heart phases becomes poor, partly due to longitudinal or T_1 relaxation of the tagging grid, and partly due to the fact that the image intensity contains a component arising from that magnetization which has relaxed since the application of the grid. This "relaxed" component, which is T_1-dependent, contains no tagging information and seriously degrades the tagging grid contrast. Thus, efficient automatic identification of the tagging grid is difficult. One motivation for tagging contrast enhancement is the need for accurate diastolic motion assessment. A second motivation for the development of an improved MRI tagging sequence is the need for a reliable computerized extraction of the motion.

The new method, called Complementary SPAtial Modulation of Magnetization (CSPAMM), separates the component of the magnetization with the tagging information from the relaxed component by performing two measurements, first with a positive and then a negative tagging grid. A conventional two-dimensional 1-1 SPAMM tagging sequence is applied to produce a positive grid; and, by inversion of one of the four RF pulses, a negative grid. The subtraction of these two measurements results in an image containing the grid, free of any contribution of the relaxed component of the magnetization. Thus, the tagging contrast is considerably enhanced.

In order to analyze the motion of the left ventricle of the heart, the reference points (4–7), usually the crosspoints of the tagging grid, have to be identified. With conventional tagging this procedure becomes difficult, as the images and the shape of the grid in the different heart phase images strongly depend on the time of acquisition and on the tagging flip angle. Therefore shape filters for the identification of the tags are required, which take the modification of the tag profiles over time into account. It is shown that the gridlines of the improved tagging sequence (7) are always represented by sharp local minima near the zero line, which makes an automatic reconstruction of the grid much easier.

In this paper we give a theoretical analysis of the tagging contrast, i.e., the contrast between the tagging grid and the untagged tissue for the conventional SPAMM technique. Theoretical conditions are derived under which the contrast may be improved and a corresponding examination technique called CSPAMM is evolved.

Following that the tagging contrast of SPAMM and CSPAMM is compared using simulations and by phantom experiments as well as by *in vivo* examinations.

THEORY AND METHOD

To compare different tagging methods, the tagging contrast is applied as an objective measure, which has relevance to the ability for the identification of the tagging grid. This tagging contrast can be defined as the ratio between the amplitude of the tagging modulation and the maximum image amplitude within a specified area of the

MRM 30:191–200 (1993)

From the Institute of Biomedical Engineering and Medical Informatics, University of Zurich, and Swiss Federal Institute of Technology, Zurich, Switzerland.

Address correspondence to: Peter Boesiger, Ph.D., Institute of Biomedical Engineering and Medical Informatics, University of Zurich and Swiss Federal Institute of Technology, Moussonstrasse 18, CH-8044 Zurich, Switzerland.

Received June 24, 1992; revised March 24, 1993; accepted April 5, 1993.

This research was supported by the Swiss Commission for the Promotion of Scientific Research (KWF).

0740-3194/93 $3.00

image. If the whole image intensity range is covered by the tagging modulation, then the tagging contrast becomes maximal; that is one. An image area without a tagging pattern has of course a minimal tagging contrast, which is zero.

Contrast in Conventional Tagging

To calculate the temporal behavior of the tagging contrast during MR imaging, we consider a series of n images acquired by a conventional multiphase imaging sequence (Fig. 1). For each image the sequence includes a slice selective excitation pulse during the application of a gradient G_z in the slice selection direction, a phase encoding gradient G_y, and a readout gradient G_x. We assume that the object to be imaged at thermal equilibrium, before any MR experiment has been performed, shows a spatial-dependent magnetization $M_0(x, y, z)$, for simplicity M_0. We denote the steady state component of the magnetization before the tagging sequence is applied by M_{ss} (x, y, z), or M_{ss}. Immediately after the application of an individual tagging sequence at the time t_0, the z-component of the spatially modulated magnetization is given by

$$M_z(t_0) = M_{ss}\,\mathrm{TAG}(x, y); \qquad [1]$$

where $\mathrm{TAG}(x, y)$ represents the modulation function. The value of the tagging function lies always in the range of $\cos\beta$ and 1, where β represents the total tagging angle. The z-magnetization immediately before the first RF imaging excitation pulse at t_1 is given by

$$M_z(t_1) = (M_{ss}\,\mathrm{TAG}(x, y) - M_0)\exp(-t_1/T_1) + M_0. \qquad [2]$$

The z-magnetization may be decomposed into two parts Q_{T1} and Q_{R1}:

$$Q_{T1} = M_{ss}\,\mathrm{TAG}(x, y)\exp(-t_1/T_1) \qquad [3]$$

$$Q_{R1} = M_0[1 - \exp(-t_1/T_1)] \qquad [4]$$

The term Q_{T1} holds the tagging information, and Q_{R1} represents an image of the object that is built up only of

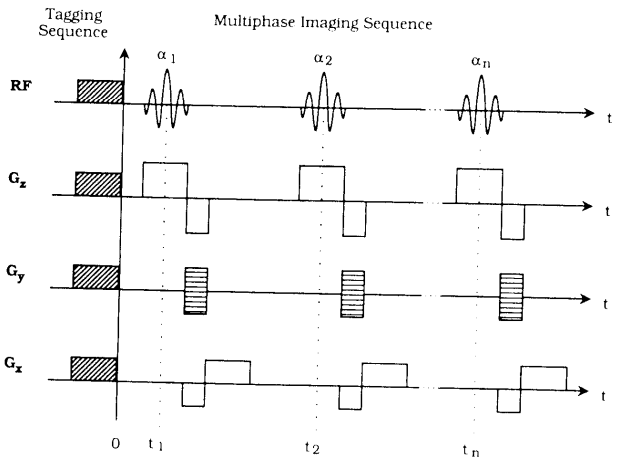

FIG. 1. Timing diagram of a typical tagging experiment. Prior to a standard multiphase imaging sequence, starting at $t = 0$, a tagging grid is applied to the tissue by a tagging sequence. The sequence for the acquisition of one image is composed of the slice selective RF excitation pulse, the slice selection gradient Gz, the phase encoding gradient Gy, and the readout gradient Gx.

that part of the magnetization, which has relaxed since the application of the tagging pattern. After the first RF imaging excitation pulse, with a flip angle of α_1, the z-magnetization is scaled by the factor of $\cos\alpha_1$. Thus, the two components of the longitudinal magnetization just before the RF excitation pulse of the kth heart phase image can be written as

$$Q_{Tk} = M_{ss}\,\mathrm{TAG}(x, y)\exp(-t_k/T_1)\prod_{j=0}^{k-1}\cos\alpha_j \qquad [5]$$

for the tagging component, and recursively

$$Q_{Rk} = (Q_{Rk-1}\cos\alpha_{k-1} - M_0)\exp(-(t_k - t_{k-1})/T_1) + M_0 \qquad [6]$$

for the relaxed term.

Immediately after the application of the tagging grid at t_0, the relaxed component is zero ($Q_{R0} = 0$), and as no RF pulse is applied $\alpha_0 = 0$. The xy-magnetization, which contributes to the kth image I_k, is that part of the sum of the tagging component Q_{Tk} and the relaxed component Q_{Rk}, which is rotated into the xy plane by the excitation angle α_k:

$$I_k = (Q_{Tk} + Q_{Rk})\sin\alpha_k. \qquad [7]$$

Equation [5] indicates that the tagging contrast decays due to longitudinal relaxation, and due to the RF excitation pulses of the imaging sequence. The component Q_{Rk} of Eq. [6] of the magnetization becomes dominant in later images of the heart cycle, especially in tissues with short longitudinal relaxation times T_1 such as fat, and does not contain any tagging information at all. Thus, this term gives an offset to the tagging grid in such a manner as to reduce the tagging contrast. In the case of a total tagging flip angle of 90°, the value of the term $\mathrm{TAG}(x, y)$ is between 0 and 1. Thus, the tagging contrast is directly given as

$$\text{tagging-contrast} = \frac{Q_{Tk}}{Q_{Tk} + Q_{Rk}}. \qquad [8]$$

Myocardial Tagging Contrast Improvement

The basic idea of the tagging contrast enhancement is to separate the term Q_{Tk} containing the tagging information (Eq. [5]) from the relaxed component Q_{Rk} of Eq. [6]. Experimentally this can be achieved by the acquisition of two images, denoted by A and B, whereby the tagging grid $\mathrm{TAG}_A(x, y)$ of image A is different from the tagging grid $\mathrm{TAG}_B(x, y)$ of image B. For simplicity assume that the steady state magnetization for both images is the same and denoted by M_{ss}. The subtraction of both kth images of the sequence leads to

$$A_k - B_k \propto M_{ss}[\mathrm{TAG}_A(x, y) - \mathrm{TAG}_B(x, y)] \exp(-t_k/T_1)\left(\prod_{j=0}^{k-1}\cos\alpha_j\right)\sin\alpha_k. \qquad [9]$$

Equation [9] shows that the relaxed term can be eliminated, and the tagging information preserved. Maximum

grid amplitude is obtained when both grids fulfill the condition

$$TAG_A(x, y) + TAG_B(x, y) = 0. \quad [10]$$

In this case the "tagged image" is

$$A_k - B_k \propto 2\, Q_{Tk}. \quad [11]$$

While the sum of the two tagging grids is zero, the addition of the signals of the two measurements leads to

$$A_k + B_k \propto 2\, Q_{Rk}, \quad [12]$$

which represents a T_1-weighted anatomical image free of any tagging information.

Experimentally two complementary tagging grids that satisfy condition [10] can be induced by two sequences of 1-1 binomial SPAMM (Fig. 2) pulses. Such sequences are composed of four nonselective RF pulses β_{x1}, β_{x2} and β_{y1}, β_{y2}, two tagging gradients G_{Tx} and G_{Ty}, which define the grid spacing and orientation, and two dephasing gradients G_{Dz1} and G_{Dz2} in the slice selection direction to despoil the remaining xy-magnetization. The longitudinal magnetization after application of the tagging pattern in the x-direction and neglecting relaxation effects is given by

$$I_z(t_3) = M_{ss}[\sin\beta_{x1} \sin\beta_{x2} \cos(\phi_x x) + \cos\beta_{x1} \cos\beta_{x2}]; \quad [13]$$

where ϕ_x depends on the tagging gradient

$$\phi_x = \gamma \int G_{Tx}\, dt. \quad [14]$$

The term ϕ_x defines the frequency of the spatial modulation. To have maximum tagging contrast the flip angles β_{x1} and β_{x2} have to be $\pm 90°$, and the sign of the tagging function depends on the signs of β_{x1} and β_{x2}. With the two excitation angles β_{x1} and β_{x2}, of + and −90°, respectively, the simple sequence can be used to generate two different grid patterns, which fulfill the condition of Eq. [10]. The transversal and the longitudinal relaxation can be neglected, as the intervals t_{Tx} and t_{Ty} for the application of the tagging gradients and t_{Dz1} and t_{Dz2} for the dephasing gradients are very short.

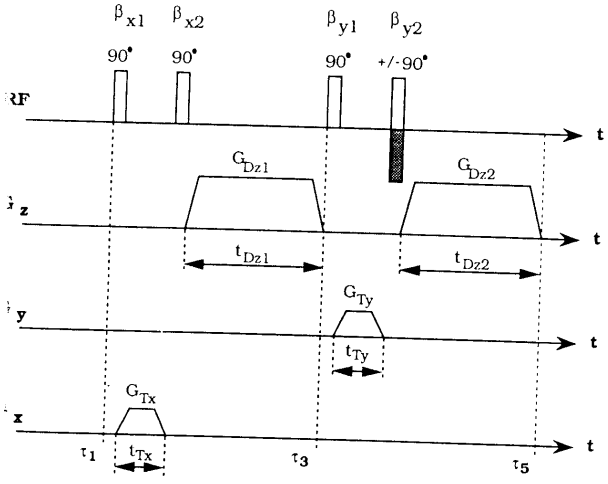

FIG. 2. Timing diagram of the CSPAMM tagging sequence. For each direction a pair of 90° RF pulses β_{x1}, β_{x2}, and β_{y1}, β_{y2} with interspersed tagging gradients G_{Tx} and G_{Ty} are used to define the grid. G_{Dz1} and G_{Dz2} are the dephasing gradients. The letters $\tau 1$ to $\tau 5$ indicate time points used in the context and the equations. To obtain a complementary tagging grid the RF pulse β_{y2} is inverted.

For calculation of the two dimensional tagging grid (Fig. 2), the two orthogonal one-dimensional tagging functions of Eq. [13] are multiplied, supposed that the magnetization in the xy-plane at time τ_3 is sufficiently dephased. For sufficient dephasing, the gradient G_{Dz1} must be strong enough relative to the slice thickness s, or more exactly

$$\phi_z = \gamma \int G_{Dz1}\, dt >> \frac{2\pi}{s}. \quad [15]$$

The two dimensional modulation of the magnetization, after the final dephasing gradient in the slice selection direction at τ_5 of Fig. 2, in good approximation can be described by

$$TAG(x, y) = \text{sign}(\beta_{y2}) \cos(\phi_x x) \cos(\phi_y y). \quad [16]$$

Again for maximum tagging contrast and to fulfill Eq. [10], β_{x1}, β_{x2} and β_{y1}, β_{y2} have to be $\pm$ 90°. The choice at which the RF pulse has to be inverted for one of the two tagging profiles is not very critical. Any one of the four pulses can show a negative sign to produce a complementary grid pattern. However, the inversion of the last RF pulse eliminates most relaxation influences arising during the tagging sequence and thus is preferred.

Optimization of the RF Imaging Excitation Pulse Angle

The tagging contrast can further be improved by optimizing the angle of the RF pulse, which is applied for the imaging procedure. The idea is to choose the imaging excitation angle for every imaged heart phase in such a manner that the xy-magnetization of the tagging grid is equal for each image of the sequence (8). The signal amplitude of the kth tagged image I_{Tk} is proportional to

$$I_{Tk} \propto M_{ss}\, TAG(x, y) \exp(-t_k/T_1) \left(\prod_{j=0}^{k-1} \cos\alpha_j \right) \sin\alpha_k. \quad [17]$$

To distribute the tagging information equally between the n images of the sequence, the condition

$$I_{Tk} = I_{Tk+1} \text{ for } k = \{1, 2, \ldots, n-1\} \quad [18]$$

has to be fulfilled. Because of the presence of the T_1 relaxation term, this can only be achieved for a single specified tissue, preferably for the myocardium with its T_1 of about 850 ms at 1.5 T (9). For investigations of the systolic heart motion, the measurements are only performed over about 30% to 60% of the cardiac cycle. The remaining 40% to 70% of the cycle are a sufficiently long magnetization recovery time, so that the last excitation angle α_n can be set to 90°. This gives a reasonable condition for the solution of the recursive Eq. [18]. For a first

approximating optimization, the steady state magnetization is not taken into account. The solution, with constant heart phase interval Δt, for the $(n\text{-}i)$th excitation angle, is

$$\alpha_{n-i} = \sin^{-1}\left(\frac{C^i}{\sqrt{\sum_{j=0}^{i} C^{2j}}}\right); \quad [19]$$

where C depends on the tissue relaxation, and is given by

$$C = \exp(-\Delta t/T_1). \quad [20]$$

Steady State Magnetization

The steady state magnetization is dependent on both the tissue relaxation and the tagging modulation function. The z-magnetization at the end of a heart cycle of period T_R can be calculated from Eq. [5] and Eq. [6]:

$$M_z(T_R) = M_{ss}\,\mathrm{TAG}(x, y)\, r_1 + R_2; \quad [21]$$

where r_1 describes the decay of the tagging information

$$r_1 = \exp(-T_R/T_1)\prod_{j=0}^{n}\cos\alpha_j; \quad [22]$$

and R_2 the relaxed term

$$R_2 = Q_{Rn}\cos\alpha_n \exp(-(T_R - t_n)/T_1) + M_0\{1 - \exp(-(T_R - t_n)/T_1)\}. \quad [23]$$

Therefore the steady state magnetization for a constant heart period T_R is

$$M_{ss}(x, y) = \frac{R_2}{1 - \mathrm{TAG}(x, y)\, r_1}. \quad [24]$$

Using CSPAMM with constant excitation pulses α_k, the steady state magnetizations for the images A and B are not equal because of the different tagging grids. These variations are the cause that the tagging grid is slightly visible in the anatomical image calculated from the relaxed component. The resident tagging grid can be removed from the anatomical images as r_1 is zero, which can be achieved by choosing the last excitation pulse angle $\alpha_n = 90°$.

SIMULATIONS

Consider a one-dimensional tagging sequence applied to a virtual phantom, which is composed of three different types of tissue. The first tissue corresponds to fat with a T_1 of 250 ms at 1.5 T (9); the second tissue has the similar characteristics as the myocardium (T_1 = 850 ms at 1.5 T); and the third tissue has the same T_1 as the myocardium but a spin density of only 70% of that of the other two tissues. This third tissue is helpful to study the shape of the tagging grid at the boundary between organs of different spin densities, such as between the myocardium and lung. However, due to susceptibility effects the signal, which can be expected from the lung, is much lower than 70% of the signal of the myocardium.

The spatial variation of the steady state magnetization due to the modulation, the influence of the imaging sequence, and the relaxation are simulated. Three image intensity profiles of modulus images, using constant excitation pulse angles of 35° and with a heart phase interval time of 150 ms, are calculated. The profile of the first image, obtained just after the application of the tagging pattern is represented by the solid line, the second by the dashed and the third by the dotted line. Before every single excitation RF pulse of the imaging sequence is applied, the xy-magnetization is completely despoiled. The duration of the entire heart cycle T_R is assumed to be 1 s.

Conventional Tagging

Using conventional tagging methods, a grid pattern with narrow stripes and high tagging and anatomical contrast is desired. The narrowness of the stripes is important to reduce the spatial error in the identification of the cross-points of the grid and for the definition of the heartwall as exactly as possible for later analysis of the motion. A binomial SPAMM sequence of higher order (3) such as a 1-2-1 sequence, or a DANTE tagging sequence (10) produces such an image whereby the grid and the anatomical details can be observed simultaneously. However, the identification of the gridlines presents some problems, which are illustrated by the following simulations.

To avoid an inversion of the modulated longitudinal magnetization in a one dimensional 1-2-1 SPAMM experiment a total tagging angle of 90° is applied (Fig. 3). The contour of the tagging profile varies strongly in the subsequent images. Additional local minima occur near the boundaries of the tissues (arrows in Fig. 3). Also the amplitude of the tagged areas is very dependent on M_{ss}, T_1, and the imaging time point. These characteristics makes an automatic detection of the tagged regions very difficult, even on a phantom that does not move. The domination of the "fat" in the third image is not because the tagging contrast is better than in the "myocardium,"

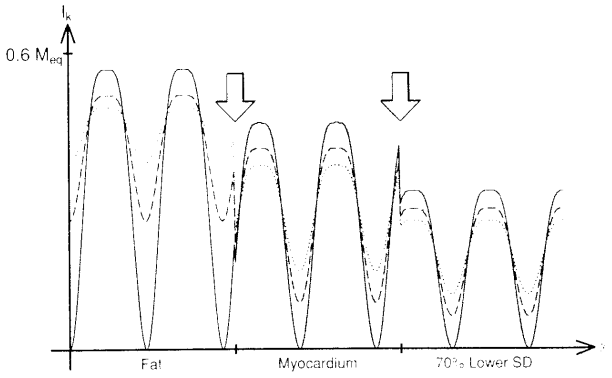

FIG. 3. Simulated 1-2-1 SPAMM image intensity profiles along the x axis through a phantom composed of three different types of tissue for a tagging angle β = 90°. The profiles are calculated for an interval time of 150 ms by 1 s of repetition time; the solid line corresponds to the first, obtained just after the application of the tagging sequence, the dashed line to the second, and the dotted line to the third image of the sequence (0, 150 ms, 300 ms), respectively.

but because the relaxed component becomes more prominent. At both tissue boundaries additional local minima can occur for different spatial offsets of the tagging grid. These additional local minima, which do not correspond to any gridline, cause errors when using automatic grid detection procedures.

When applying a tagging angle greater than 90° (for instance to increase the tagging contrast in the myocardium for the third, in this case the systolic image), the evaluation of the tagging grid becomes even more difficult, because one has to decide whether the magnetization of the bright image areas has been inverted or not. This problem is illustrated in Fig. 4, where a tagging angle of 140° is applied. Here, not every local minimum can be related to a gridline. Dependent on tissue and time of the image acquisition some local maxima can correspond to a gridline. The profile differences at the various imaging times make a fully automatic detection of the tagged region even more difficult.

Improved Tagging Contrast

Figure 5 shows the results of the simulation of the CSPAMM sequence with β_{x1}, β_{x2}, $\beta_{y1} = 90°$ and $\beta_{y2} = \pm 90°$. On the three images at different times the shape of the tagging profile remains the same, apart from tissue dependent amplitude variations. The influence of the tissue parameters M_{ss} and T_1 also modifies the shape of the profile, but do not influence the amplitude of the minima of the gridlines, which is zero for all images of the sequence.

Additional local minima may also appear at both tissue boundaries (e.g., third image, boundary fat-myocardium), but their amplitude is greater than the amplitude of those local minima corresponding to the gridlines. Because the gridlines are always represented by local minima near the zero line, the development of a procedure for the identification of these lines becomes relatively simple.

For the computerized evaluation it is not necessary to use modulus images only. With CSPAMM there is no offset to the gridlines. Thus, the search can be performed on the real and imaginary part of the images. This doubles the signal-to-noise ratio compared with the conventional SPAMM technique; and also the tracking of the grid is easier because of the positive and negative checker board pattern on the image.

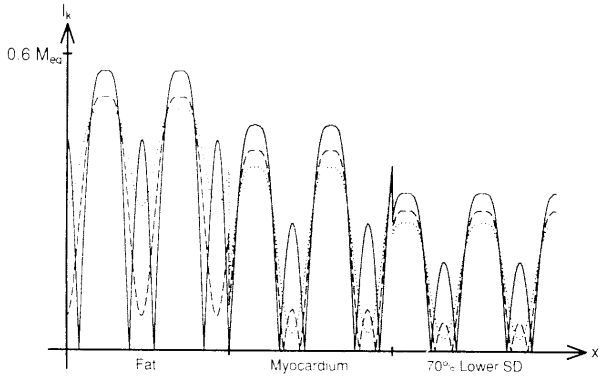

FIG. 4. Simulated 1-2-1 SPAMM image intensity profile for a total tagging angle $\beta = 140°$. The same phantom and imaging parameters as described in Fig. 3 are used.

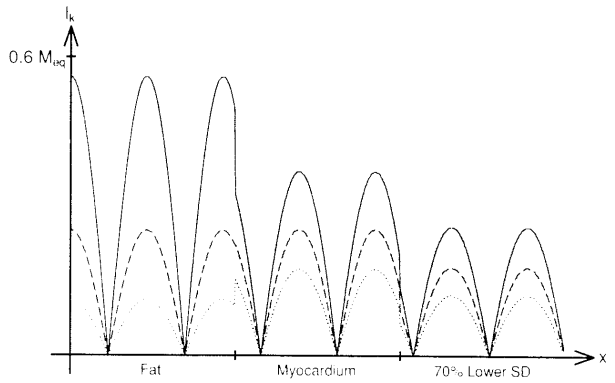

FIG. 5. Simulated CSPAMM image profiles of the phantom described in Fig. 3 using constant imaging excitation angles of $\alpha = 35°$.

Tagging Contrast for Optimized RF Imaging Excitation Pulse Angles

Figure 6 shows the amplitude of the tagging grid relative to the steady state magnetization for $n = 10$ images acquired with a time interval of 100 ms. These tagged parts of the magnetization for constant (dashed lines, empty symbols) and for optimized excitation pulses using Eq. [19] (solid line, filled symbols) are calculated for three different types of tissue—fat (△, ▲), water (◇, ◆), and the myocardium (○, ●). Using constant excitation angles, the tagging amplitude, and thus the signal-to-noise ratio of the images, decreases with the number of excitations for all types of tissue, being more severe for those with lower T_1 values. The tagging amplitude in the myocardium using optimized excitation pulse angles is constant. Therefore, the signal-to-noise ratio in the later images is considerably increased. With the optimized sequence the steady state magnetization is lower compared with

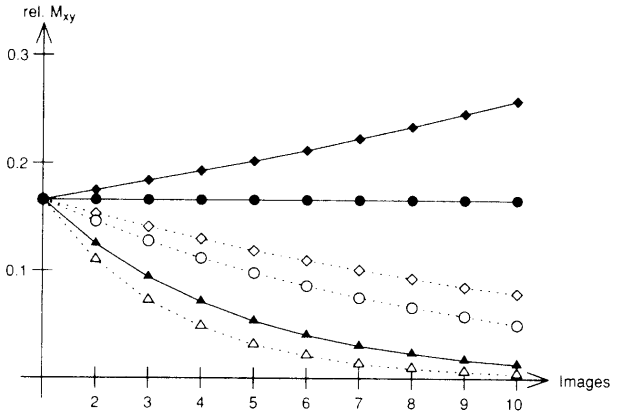

FIG. 6. Simulated amplitudes of the tagged magnetization relative to the steady state magnetization of 10 tagging images using constant (dashed lines, empty symbols) and optimized (solid lines, filled symbols) RF excitation pulse angles. Three different tissues (different T_1), such as fat (triangles), water (squares), and myocardium (circles), are compared. The time interval between subsequent images is 100 ms.

the sequence with constant excitation pulses. However, for myocardial tagging experiments the improvement of the signal-to-noise ratio is evident (compare Figs. 5 and 7). As a consequence of the 90° excitation pulse for the last image of the sequence, the steady state magnetization is no longer dependent on the spatial modulation.

Figure 7 shows a simulation of the same one-dimensional phantom and with the same parameters as used in Figs. 3 through 5, but with the optimized excitation angles. The tagging contrast in the myocardium and in the tissues with the same T_1 is equal for all images.

As the amplitude of the tagged component is proportional to the steady state magnetization, one could in principle optimize the amplitude of the steady state magnetization by modification of the angle of the last excitation pulse. However, for practical reasons such as the variation of the repetition time due to ECG-triggering and the alternating tagging pattern, which influence the steady state magnetization, the choice of the last excitation angle less than 90° will not increase the image quality significantly. Further, to gain anatomical images, which are completely free of the tagging grid, and to avoid interference with the actual tagging grid and the grids of subsequent heart cycles, the last excitation angle has to be 90°.

Comparison Between Conventional and Improved Tagging

The tagging contrast of any conventional tagging technique, such as SPAMM, is only maximal (tagging contrast = 1) for one specified heart phase image by choosing the total tagging angle in such a way that the magnetization of the gridlines becomes zero for a known tissue such as the myocardium. The tagging contrast for later images decreases exponentially toward zero. The tagging contrast in earlier modulus images is also lower than one due to the inversion of the grid lines. Those inversions are a main problem, when automatic grid line detection algorithms are used. The tagging contrast when using CSPAMM is maximal for every image through the entire heart cycle as the whole range of image brightness is utilized by the tagging pattern. Of course the absolute amplitude of the tagged component of the magnetization decreases also exponentially with T_1.

The higher the order of a binomial SPAMM sequence the narrower the stripes get and the more the anatomical details become visible. Therefore, using conventional tagging techniques 1-2-1 or even 1-3-3-1 SPAMM sequences generally are preferred to 1-1 SPAMM sequences.

However, for CSPAMM in modulus images the shape of the 1-1 pattern, given as $|\cos(\phi_x x)|$, is not much different from the pattern that is generated by a 1-2-1 pulse for SPAMM. Figure 8 shows the direct comparison between both tagging patterns obtained immediately after the application of the spatial modulation. The solid line describes the tagging profile of the CSPAMM method, and the dashed line the shape of the 1-2-1 SPAMM sequence with a total tagging angle of 90°. It is evident that the stripes are slightly narrower for the 1-1 CSPAMM sequence and that the nontagged area is a little larger and flatter for the 1-2-1 SPAMM sequence.

For *in vivo* measurements the application of the tagging grid and imaging procedure are synchronized to the ECG. During the short time interval between the R-wave and the onset of the motion the tagging sequence has to be applied and the first image has to be acquired. Therefore, the tagging sequence has to be as compact as possible. The 1-1 CSPAMM sequence fulfills this requirement much better than most other methods, such as the higher order SPAMM (3), the *k*-space trajectory method (11), the chessboard (12) DANTE (10) sequences, or to the tagged saturation stripes method (13). Compared, e.g., with a conventional SPAMM sequence, the tagging gradients G_{Tx} and G_{Ty} only require half of the duration to obtain the same grid spacing.

EXPERIMENTAL RESULTS

The CSPAMM and the 1-2-1 SPAMM sequence were implemented on a commercial 1.5 T MR-imaging system (Philips Gyroscan S15HP, Philips Medical Systems, Best, The Netherlands). Both sequences were applied prior to a standard gradient echo imaging sequence (14). Due to the limitations of the pulse program circuit of the system,

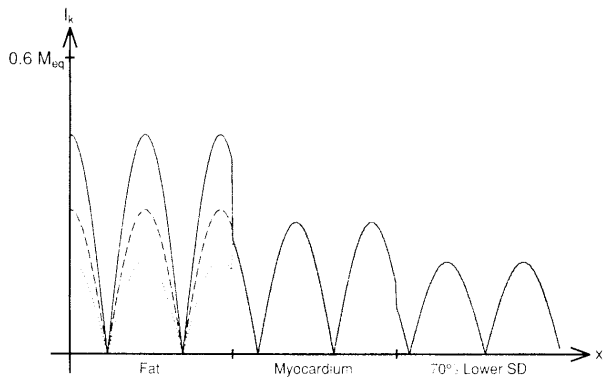

FIG. 7. Simulated CSPAMM image profiles using the same tagging and imaging parameters as for the simulation of Fig. 5 except the imaging excitation pulse angles. Those angles were chosen according to Eq. [18] for a T_1 of 850 ms.

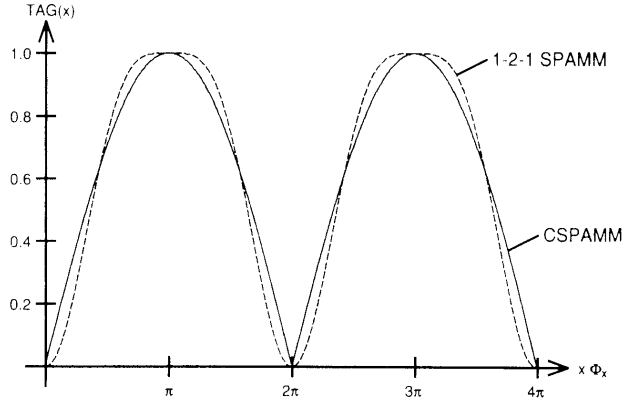

FIG. 8. Tagging profile comparison of the 1-2-1 SPAMM (dashed line) tagging function with a total tagging flip angle of 90° and the CSPAMM (solid line) tagging function in a modulus image.

the excitation pulse angles of the imaging sequence $\alpha_i = \alpha$ were constant for every heart phase and not optimized according to Eq. [19]. It was chosen as a function of the total number of heart phases n,

$$\alpha = \sin^{-1}\left[\frac{1}{\sqrt{n}}\right]; \qquad [25]$$

which is the angle that produces optimal tagging contrast in the last image. (The tagging contrast of the preceding images is better than for the last image.)

Phantom Results

For the experimental comparison of the two tagging methods (SPAMM, CSPAMM), a two-compartment phantom was used with solutions of different $MnSO_4$ concentrations and thus with different T_1 relaxation times. For the left compartment, a solution with a T_1 of 250 ms, which is approximately the same as the T_1 of fat, was chosen. The right compartment emulates the myocardial tissue with a T_1 of about 850 ms (9). The parameters for the phantom measurements are 256 × 256 mm FOV with a scan resolution of 256 × 512 and a 5-mm slice thickness. Five images using the system's headcoil are acquired at 50, 200, 350, 500, and 650 ms after the application of the tagging grid. According to Eq. [25], the imaging excitation RF pulse angle was 27° for all heart phases. The repetition time of the whole sequence was 1000 ms.

The results of the 1-2-1 SPAMM and the 1-1 CSPAMM tagging method are compared in Fig. 9. The left row refers to the five 1-2-1 SPAMM images, the intermediate and the right rows present the tagged and the "anatomical" images, which are acquired simultaneously with the CSPAMM sequence.

The tagging contrast and also the pattern of the modulated structures of a 1-2-1 SPAMM tagging grid is dependent on the time of the image acquisition. The five SPAMM images cannot be transformed from one into another by a simple scaling function, because the tagging contrast strongly depends on tissue and time. As the tagging angle is 140° to improve the tagging contrast for later heart phase images, the gridlines mainly in the first but also in the second modulus image are inverted, because of the negative z-magnetization. In the third image, which can be compared with an *in vivo* systolic image, the tagging contrast becomes maximal for the solution emulating the myocardium, as the z-magnetization for the gridlines, except at the crosspoint, is nearly zero. In the last two images, the gridlines become brighter, and the tagging contrast decreases. The scaling of the image brightness is usually determinated by the brightest zones of the image, which are usually those with the shortest longitudinal relaxation such as fat.

Because the two dimensional tagging function is the multiplication of two one-dimensional modulation functions, the intersection points of the tagging grid always have a positive z-magnetization. This is apparent in that the grid intersection points are always represented as local maxima, which cause further problems for an automatic crosspoint detection procedure.

For CSPAMM the contrast and the pattern of the tagging grid, (middle row) is nearly stable in the myocardium like area of the phantom for all images of the sequence. The improvement of the tagging contrast is evident, as the whole range of the image gray scale is utilized by the tagging function. The gridlines as well as the intersection points always appear as local minima near the zero line. Because the signal amplitude decreases when using constant excitation RF pulses, the signal-to-noise ratio becomes progressively worse. The tagging grid in the phantom area with approximately the same T_1 as fat fades faster than the grid in the other region of the phantom. Thus tissue with shorter T_1 as the T_1 of the myocardium becomes suppressed in the images induced by the tagged component of the magnetization as

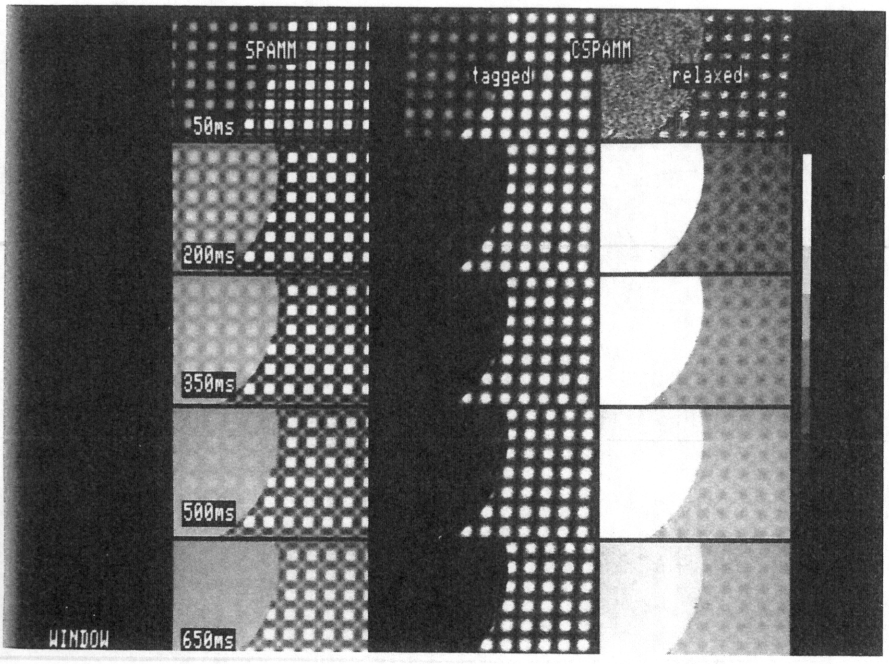

FIG. 9. Multiphase measurements on a two-compartment phantom using a 1-2-1 SPAMM sequence with a tagging angle of 140° (left row) and the CSPAMM method, where the image of the tagged (middle row) and the relaxed (right row) magnetization component is reconstructed. The time interval between subsequent images is 150 ms.

the ratio of the tagged and the relaxed component of the magnetization decreases faster than in the myocardium.

The relaxed images of CSPAMM as they are produced by addition of the two corresponding data sets are progressively T_1-weighted images. They can be used for tissue characterization; with the exception of the first image, which is obtained just after the application of the tagging grid, when very little magnetization has relaxed. However, low intensity tagging grid structure can be observed, especially in the myocardium-like area. The reason for this structure lies in the small difference of the steady state magnetization of the positive and negative tagging grid.

Human *in Vivo* Results

The measurements on human volunteers, performed using the system's body coil, were located by double angulation perpendicular to the long axis of the heart (short axis view). The field of view was 400 mm with a scan resolution of 128 × 256 and slice thickness of 8 mm with four averages, in order to realize the same examination time for both the conventional 1-2-1 SPAMM sequence and the 1-1 CSPAMM sequence. To reduce the blood flow artefacts, two slice selective saturation pulses were applied with a slice thickness of 60 mm and a separation to the measured slice of 10 mm.

Figure 10 shows the comparison of the two *in vivo* measurements of the same healthy volunteer. The image (a) is obtained using the 1-2-1 SPAMM tagging sequence with a tagging angle of 140°. The tagged and the relaxed component of the images are superimposed and can hardly be separated by image processing procedures. The two right images are acquired using CSPAMM. The image containing the tagging grid and the anatomical image are separately reconstructed using the same two *k*-space data sets. Image (b) of the tagged component is the Fourier transform of the difference of the two *k*-space data sets where the image (c) of the relaxed magnetization component refers to the sum of the *k*-space profiles.

The darkest objects in the SPAMM image are not the gridlines but the low signal objects, such as the lung tissue and air-filled structures. The image brightness is scaled between these low signal objects and the brightest objects, which are the fat regions. Because of the short T_1 of fat, the relaxed component of the magnetization is here dominant. The darkest structures on the CSPAMM images are the tagged grid lines and the objects with low signal. The brightest image areas correspond to tissue with the same or longer T_1 than the myocardium. Therefore, the tagging contrast is maximal. The CSPAMM tagged image appears noisier because the relaxed component of the image has been eliminated and the remaining signal is scaled to the whole range of the image brightness.

As a by-product of the CSPAMM method, the signals of the fat tissue are suppressed. Thus, chemical shift displacement, which results to an initial deformation of the tagging grid, presents no longer problems.

The image of the relaxed component shows a good T_1 contrast, which also allows study of the fat regions around the heart. The contrast between the myocardium and the blood within the ventricles, however, is poor, because their T_1 times are nearly equal.

Figure 11 shows the measured tagging contrast of SPAMM (■) and CSPAMM (▲) (same measurement as for Fig. 10) of the four heart phase images in comparison with the simulated values according to Eq. [8]. The tagging contrast was measured in a manually selected region of interest within the septal, the anterior, the lateral, and the inferior segment of the myocardium. The tagging contrast values of the four segments were averaged for every heart phase image. The measured values for SPAMM show the drastic decay of the tagging contrast in good coincidence with the theory (solid line). The tagging contrast for CSPAMM is constant for all heart phases. The difference of about 5% according to the theoretically expected tagging contrast of one (dashed line) is due to the modulus function of the image reconstruction, due to the integration of the signal over an image pixel, and due to the noise.

When using conventional SPAMM tagging techniques only the systolic motion can be observed (15) in contrast to CSPAMM; Fig. 12 shows a set of five tagged apical heart phase images of a patient with an infarction in the anterior segment almost throughout the entire cardiac cycle. The images are measured starting 40 ms after the detection of the R-wave of the ECG with a time interval between the images of 155 ms. The third image is obtained at end systole. The last image is measured 660 ms after the R-wave at diastole. The grid on all tagged images is clearly visible. However, because the excitation angle of the imaging sequence was constant here (27°), the signal-to-noise ratio decreases for later images, which can be circumvented if the imaging excitation angles α_i are optimized according to Eq. [19]. The result shows that the CSPAMM tagging technique can be used to observe as well the diastolic cardiac motion with the same high accuracy as the systolic contraction.

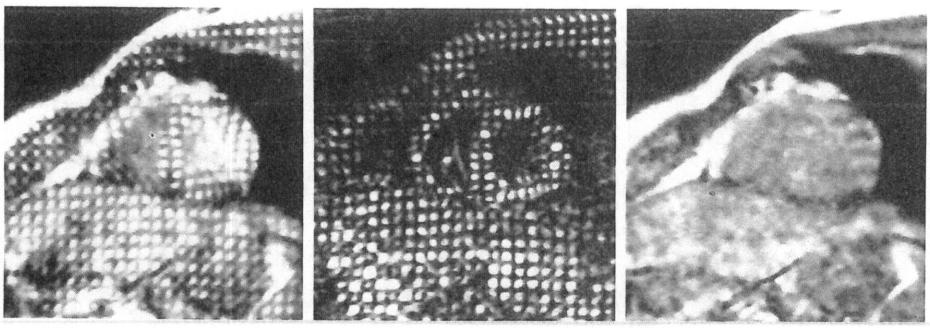

FIG. 10. Comparison between a systolic 1-2-1 SPAMM image (left) with a tagging angle of 140° and the systolic CSPAMM images (tagged: middle, relaxed: right) of the same heart short axis slice of a healthy volunteer.

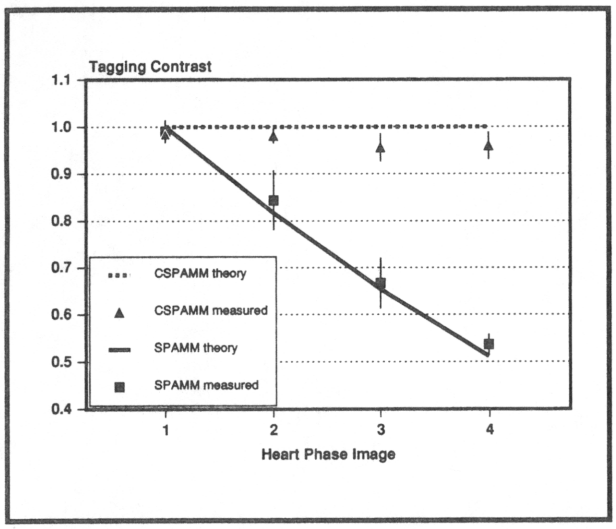

FIG. 11. Experimental tagging contrast for SPAMM (squares) and CSPAMM (triangles) for the measurements shown in Fig. 10 for all of the four heart phases. The tagging contrast is plotted as an averaged value of the contrast within the septal, the anterior, the lateral, and the inferior segments of the myocardium. The results are compared with simulations according to Eq. [8].

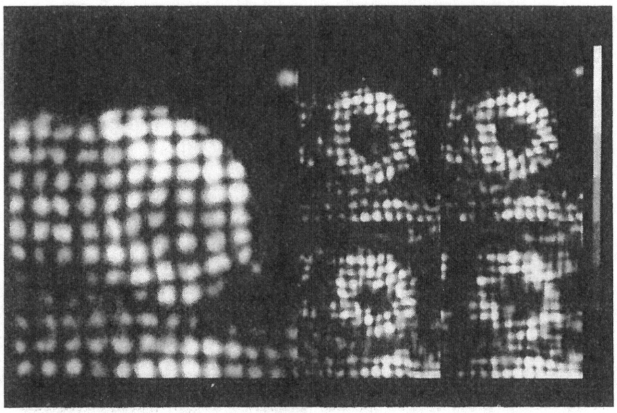

FIG. 12. Five apical, short axis, tagged CSPAMM images from end diastole to end systole and to diastole. The first image (left) is acquired just after the application of the tagging sequence, the third image represents the end systole and the last image is measured 620 ms after the application of the tagging grid.

CONCLUSIONS

The optimum tagging grid for an automatic grid line and crosspoint detection is a grid without anatomical contrast but with grid deformations, which are only induced by in-plane motion. The optimum image for the identification of the heartwall is an image without any grid information. The CSPAMM tagging method comes very close to the satisfaction of these requirements.

For the assessment of the cardiac motion, a tagging grid is required, which is not deformed by the tissue parameters, such as relaxation or chemical shift displacement, and by through-plane motion. The CSPAMM method completely suppresses the grid pattern deformation due to T_1 relaxation and also the displacement of the grid (chemical shift) in fat tissue, which is often a problem when measuring patients with infarctions at the late phases of the cardiac cycle.

The fact that the gridlines are represented by local minima near the zero line makes a strategy for an improvement of the signal-to-noise ratio possible. When using a one-dimensional tagging sequence, where the tagging gradient has the same direction as the readout gradient of the imaging sequence, only a limited number of *k*-space profiles, e.g., as low as 64, are required to reconstruct the stripe pattern. Two such CSPAMM images, with their readout direction orthogonal to each other, can be multiplied to obtain a two-dimensional tagging grid. The acquisition can be performed within 256 heart beats. Compared with an image of two averages and 128 profiles, the signal-to-noise ratio is significantly improved.

The fading of the tags and the difficult motion analysis by pattern recognition algorithms are discussed as the main problems in myocardial tagging experiments (15, 16). The improved tagging contrast when using CSPAMM allows one to study not only the motion from end diastole to end systole but also the diastolic motion within the same multiheart phase imaging cycle. The segmentation of the tagging grid in CSPAMM images can be done with a simple minima search perpendicular to the gridlines in addition with the condition that the local minima representing the gridline are near the zero line. In contrast to motion analysis by phase contrast (16), the displacement is directly measured using robust modulus images without velocity integration and velocity quantification problems. However, a low signal from the lung, the disturbed blood flow within the ventricles, and the noncontinuous motion along tissue boundaries still provide various challenges to a fully automatic detection of the gridlines and the intersection points of the grid at this time.

It may seem to be a disadvantage of the new tagging method that at least two measurements have to be performed. However, in our experience, with conventional *in vivo* tagging, usually two or even four measurements are required to reduce sufficiently motion and arrhythmia artefacts. As the sum of the positive and the negative tagging grid generated with the 1-1 SPAMM sequence is zero, an anatomical image, free of the tagging component, can additionally be calculated by adding the two measurements. The "gratis" anatomical images are useful in that the epicardium and endocardium can be determined much more precisely than this is possible from the tagged images, where the dark stripes often mask the actual boundary of the heart wall.

ACKNOWLEDGMENTS

The authors thank Professor H. P. Krayenbuhl and Professor O. Hess of the Cardiology Department of the University Hospital Zurich, for helpful discussions; Mrs. E. Niederer, for care of the volunteers and the patients during MRI examinations; and Philips Medical Systems, Best NL, for technical support.

REFERENCES

1. E. A. Zerhouni, D. M. Parish, W. J. Rogers, A. Yang, E. P. Shapiro, *Radiology* **169,** 59 (1988).
2. L. Axel, L. Dougherty, *Radiology* **171,** 841 (1989).

3. L. Axel, L. Dougherty, *Radiology* **172,** 349 (1989).
4. L. Axel, *in* "Book of Abstracts, 9th Annual Meeting, Society of Magnetic Resonance in Medicine, 1990," p. 279.
5. S. E. Maier, S. E. Fischer, G. McKinnon, O. M. Hess, H. P. Krayenbühl, P. Boesiger, *Comput. Med. Imaging Graphics* **16(2),** 73 (1992).
6. S. E. Fischer, G. McKinnon, S. E. Maier, P. Boesiger, *in* "Book of Abstracts, 10th Annual Meeting, Society of Magnetic Resonance in Medicine, 1991," p. 16.
7. P. Boesiger, S. E. Fischer, O. M. Hess, H. P. Krayenbühl, S. E. Maier, G. McKinnon, *MedicaMundi* **36(2),** 106 (1991).
8. P. A. Bottomley, T. H. Foster, R. E. Argersinger, L. M. Pfeifer, *Med. Phys.* **11(4),** 425 (1984).
9. P. Mansfield, *Magn. Reson. Med.* **1,** 370 (1984).
10. T. J. Mosher, M. B. Smith, *Magn. Reson. Med.* **15,** 334 (1990).
11. T. G. Reese, J. D. Pearlman, *in* "Book of Abstracts, 9th Annual Meeting, Society of Magnetic Resonance in Medicine, 1990," p. 268.
12. C. Thomsen, J. Møgelvang, Q. Peng, *in* "Book of Abstracts, 9th Annual Meeting, Society of Magnetic Resonance in Medicine, 1990," p. 689.
13. B. D. Bolster, E. R. McVeight, E. A. Zerhouni, *Radiology* **177,** 769 (1990).
14. P. van der Meulen, J. P. Groen, A. M. C. Tinus, G. Bruntink, *Magn. Reson. Imaging* **6,** 355 (1988).
15. L. Axel, *in* "Book of Abstracts, 10th Annual Meeting, Society of Magnetic Resonance in Medicine, 1991" p. 13.
16. R. Pelc, *in* "Book of Abstracts, 10th Annual Meeting, Society of Magnetic Resonance in Medicine, 1991," p. 17.